Steady flow instability in an annulus with deflectors at rotational vibration

Nikolai V Kozlov, Dominique Pareau, Andrei O Ivantsov, Moncef Stambouli

Steady flow instability in annulus with deflectors at rotational vibration

Nikolai V. Kozlov[1,2]‡, Dominique Pareau[3], Andrei O. Ivantsov[4] and Moncef Stambouli[3]

[1]Lab. Vibrational Hydromechanics, Perm State-Humanitarian Pedagogical University, Perm, Russia
[2]Lab. Hydrodynamic Stability, Institute of Continuous Media Mechanics UB RAS, Perm, Russia
[3]Lab. Chemical Engineering, École Centrale Paris, Châtenay-Malabry, France
[4]Lab. Computational Hydrodynamics, Institute of Continuous Media Mechanics UB RAS, Perm, Russia

Abstract. Experimental study and direct numerical simulation of dynamics of an isothermal low-viscosity fluid are done in a coaxial gap of a cylindrical container making rotational vibrations relative to its axis. On the inner surface of the outer wall of the container, semicircular deflectors are placed regularly, playing the role of flow activators. As a result of vibrations, the activators oscillate tangentially. In the simulation a two-dimensional configuration is considered, excluding the end-wall effects. In the experiment a container with large aspect ratio is used. Steady streaming is generated in the viscous boundary layers on the activators. On each of the latter, beyond the viscous domain, a symmetric vortices pair is formed. The steady streaming in the annulus has an azimuthal periodicity. With an increase in the vibration intensity, a competition between the vortices occurs, as a result of which one of the vortices (let us call it even) approaches the activator and the other one (odd) rolls away and couples with the vortices from the neighbouring pairs. Streamlines of the odd vortices close on each other, forming a flow of a cog-wheel shape that encircles the inner wall. Comparison of the experiment and the simulation reveals an agreement at moderate vibration intensity.

Keywords: Mixing, Mass Transport, Annulus, Rotational Vibration

‡ Corresponding author: kozlov.n@icmm.ru

1. Introduction

Vibration is an efficient instrument for control of mechanical systems (Blechman 2003) and it brings multiple advantages and new solutions to technological processes. A remarkable effect due to vibration in fluid systems is the steady streaming, which found its application in diverse areas (Riley 2001).

A problem of mixing and homogenization of solutions in chemical and biological reactors is vital for efficient mass transfer. For instance, traditionally a rotating stirrer is used for agitating a liquid solution. This technique can be very efficient in terms of homogenization at high rotation rates. But it has some drawbacks, for example high energy consumption. In the case of multiple phases, one of the disadvantages is interface destabilization, which creates difficulties in controlling the chemical reaction rate. And in biological systems it is high shear stress, which is harmful for living organisms like microalgae. An approach to deal with agitation in a reactor is based on the use of vibration-induced streaming. For instance, introducing vibrating activators in a chemical cell with constant interface has demonstrated promising results based on a heat transfer study (Ivanova *et al* 2009).

The study of transport of sub-micron sized particles in the acinar region of the lung revealed that the steady streaming is at the origin of kinematic mixing in the alveolus (Kumar *et al* 2011). Steady streaming may also be used for enhancement of the separation process, in which it allows the reduction of membrane fouling. So, Kola *et al* (2012) successfully applied the transversal vibrations to a system with cylindrical hollow-fibre membrane.

The flow around an oscillating cylinder has been an object of interest for many researchers. Schlichting (1932) studied theoretically and experimentally the flow around a circular cylinder oscillating along its diameter. He found that a steady streaming is generated in the Stokes layers on the surface of the cylinder and that a secondary steady streaming is excited outside these viscous boundary layers. Stuart (1966) theoretically showed that at a large characteristic Reynolds number, an outer boundary layer appears within which the steady-streaming velocity decays to zero. Honji (1981) experimentally found a three-dimensional streaked flow around an oscillating cylinder developing due to an instability. A systematic experimental study of different flow regimes around an oscillating cylinder was performed by Tatsuno and Bearman (1990) in a quite large range of Keulegan–Carpenter numbers.

The use of rotational vibrations brings an advantage in controlling the shear stress, since the flow is mainly tangential to the container walls and eventual deflectors. Another advantage is the possibility of producing homogeneous mixing of the solution by the means of shaping the container walls according to some regular pattern.

Vibrational flows can be highly disturbed and the study of their stability is an important problem for optimization of operational regimes of vibratory devices. In the present work an experimental and numerical study is done of the fluid flow in an annulus with deflectors regularly situated on the outer wall. The considered apparatus represents

a conception of liquid mixing via rotational vibrations.

2. Experimental setup

The working volume is formed by two coaxial cylinders. The inner and outer radii of the annulus are, respectively, $R_\mathrm{i} = 30.0$ mm and $R_\mathrm{o} = 50.0$ mm (Fig. 1*a*). The interior height of the cell equals 200.0 mm. On the interior surface of the outer cylindrical wall, six deflectors with the shape of half-cylinders of diameter $d = 16.0$ mm are placed equidistantially. They serve as flow activators.

A photo of the experimental setup is shown in Fig. 1*b* and a scheme of the vibrator is presented in Fig. 1*c*. The transparent cylindrical container *1* with an annular cavity is fixed on the vibrating platform *2* and filled with a working liquid. The stepper motor McLennan 34HSX-208 *3* transmits rotation to the crank *4* via a belt drive *5*. The motor is controlled by the drive MSE570-2. The connecting rod *6* transforms rotation of the crank into rotational oscillations of the platform and the cavity. The vibration frequency f varies from 0 to 20 Hz. The DC alimentation of the motor is done with the help of a power supply Isotech IPS 303DD. When a higher intensity of vibration is needed, two power supplies are connected in a series. The clock signal for the motor is provided by a sound generator Hameg HM8150. The angular amplitude of vibration is set by positioning a crank pin *7* and varies in the range $\varphi_0 = 0.05 - 0.2$ rad. The vibration amplitude is measured optically; for this, a laser *8* is fixed on the vibrating platform. The laser beam is projected on a screen *9* and the length of the laser track is measured. In the studied range of parameters f and φ_0 the motion of the vibrating platform remains sinusoidal.

The working fluid was water, into which a small amount of tracer particles Rilsan D40 (with the diameter of 40 μm) was added. Laser light sheet was used for particles illumination. The images were captured using a Dantec CCD camera FlowSense 2M and processed for PIV (Particle Image Velocimetry) with PIVlab software (Thielicke and Stamhuis 2014). PIV technique was adapted for studying a steady streaming: the images were taken with the frequency of vibration. Consequently, they were all in the same phase. The time step for each image pair was taken equal to the period of vibration. For higher precision, velocity field obtained through PIV was averaged over 50 image pairs. Each image pair was processed in three consecutive passes with gradual decrease in the size of interrogation area: 64×64, 32×32, 16×16 pixels.

3. Numerical method

Direct numerical simulation (DNS) of the flow was done in a software package ANSYS Fluent. A two-dimensional transient-time formulation was used. Pressure and velocity were coupled. The spatial descretization was done using the model PRESTO! for pressure and the third-order MUSCL scheme for momentum. For temporal discretization a second order implicit formulation was chosen. Rotational

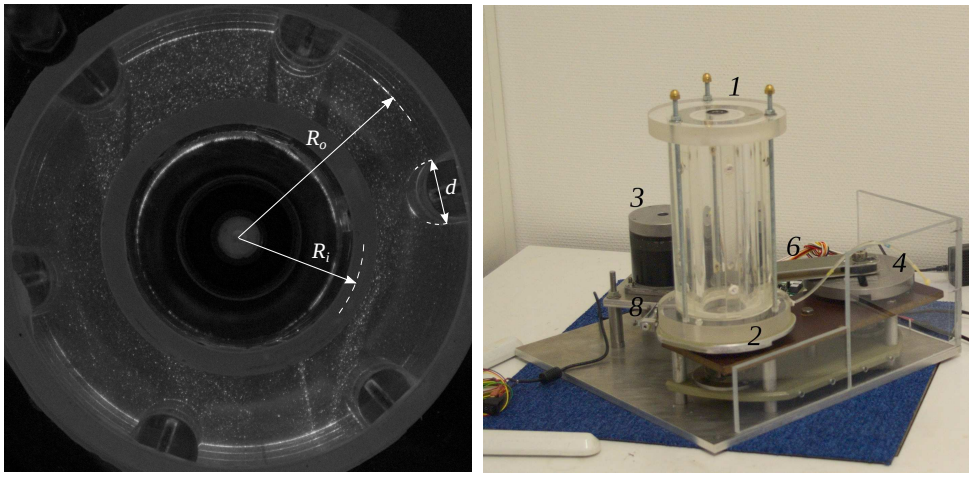

a *b*

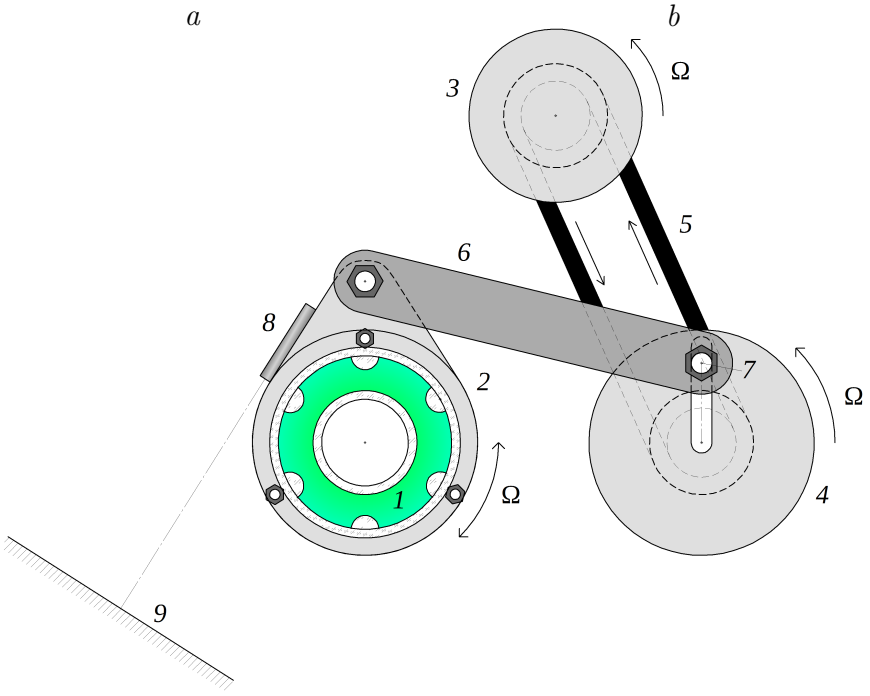

c

Figure 1. Experimental setup. *a* – Photograph of the annulus through the upper lid, along the axis of rotation; the dimensions are depicted in the plane of the laser light sheet. *b* – Experimental cell mounted on the vibrator. *c* – Scheme of the vibrator: *1* – cell with annulus, *2* – vibrating platform, *3* – stepper motor, *4* – crank, *5* – belt drive, *6* – connecting rod, *7* – crank pin, *8* – laser, *9* – screen

vibrations and time averaging of solution were done through the user defined functions (UDF). The time step was equal to $\frac{1}{100}$ of the oscillation period, $\tau = T/100$. The frame rotation at a constant rate was imposed. These parameters correspond to the following Navier-Stokes equation:

$$\frac{\partial \mathbf{v}}{\partial t} + \nabla\left(\mathbf{v}_{\mathrm{r}}\mathbf{v}\right) + \mathbf{\Omega}_{\mathrm{r}} \times \mathbf{v} = -\nabla p + \nu\Delta\mathbf{v}$$

Here, p stands for pressure, ν is the fluid kinematic viscosity. $\mathbf{v}_{\mathrm{r}}$ is the fluid velocity in the rotating reference frame:

$$\mathbf{v}_{\mathrm{r}} = \mathbf{v} - \mathbf{\Omega}_{\mathrm{r}} \times \mathbf{r}.$$

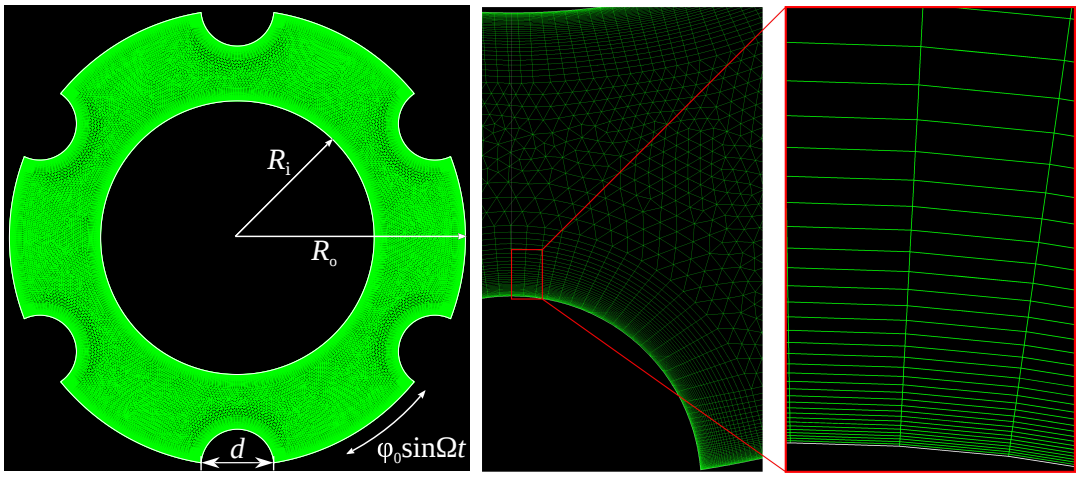

Figure 2. Annulus with deflectors with the grid meshed for the frequency 4 Hz (a); R_{i} – inner radius, R_{o} – outer radius, d – activator diameter. The figure (b) is zoomed: adaptive mesh is seen in the boundary zone on the walls

The angular rotation rate $\mathbf{\Omega}_{\mathrm{r}}$ was substituted through the UDF by a harmonic function

$$\mathbf{\Omega}_{\mathrm{r}} = \mathbf{k}\varphi_0 \cos\Omega t.$$

Here, $\mathbf{k}$ is the axial unit vector, and $\Omega = 2\pi f$.

The fluid velocity was averaged over a period of oscillations, i.e. each 100 time steps.

For the working fluid, the properties of water were used. The laminar viscous model was chosen. Since the fluid is low-viscosity, viscous interaction takes place in thin Stokes boundary layers of the thickness $\delta = \sqrt{2\nu/\Omega}$ near the solid walls. In order to have an appropriate resolution of the boundary layers, an adaptive mesh was used (Fig. 2). The regions near the walls (viscous domain) were meshed with quasi-rectangular cells of constant azimuthal dimension and with progressively increasing radial thickness. The thickness of the first cell was calculated as $\delta/25$, the increment factor was 1.1, the number of cells in the boundary zone was taken such as to cover the thickness of $\frac{3}{20}$

of the annulus width ($R_o - R_i$). The azimuthal size of the cells on the wall was taken as $\frac{1}{50}$ of the activator circumferential length. The region outside the boundary zone (non-viscous domain) was meshed with triangular cells with the average size equal to $\frac{1}{40}$ of the annulus width.

The numerical method was tested with finer boundary zone meshing, with the thickness of the first cell $\delta/40$. The time-averaged flow velocity discrepancy was only 0.07%. This allows us to consider that the thickness of the first cell equal to $\delta/25$ is sufficient.

4. Steady streaming

Rotational vibration creates tangential oscillations of the cavity wall relative to the fluid. Part of the fluid is displaced by oscillating activators, which move together with the cavity wall. Since the width of the annulus is not constant, narrower at activators, the azimuthal gradient of the pulsation velocity amplitude appears. In these conditions, fluid oscillations lead to the generation of average flows in the thin oscillating boundary layers near the walls (Schlichting 1968). This mechanism is known as steady streaming (Batchelor 1970). The average mass force acting in the boundary layers involves fluid in the whole layer in a steady motion of vibrational nature.

4.1. Experimental results

At vibration, on the background of oscillatory motion, a steady streaming is generated, and a periodic average vortex pattern is formed in the annulus (Fig. 3). Each vortex is in contact with an activator and washes its surface in the outward direction (with respect to the container axis). At equal distance from two neighbouring activators the vortices come into contact and are directed inward. The spatial period of vortex pattern is equal to the period of activators positioning. On a single activator two vortices are counter-rotating (Fig. 3*a*, *1*). Besides, a pair of minor vortices is generated on the opposite side, near the inner wall (Fig. 3*a*, *2*). Another pair of minor vortices is formed on the outer wall between the activators (Fig. 3*a*, *3*).

The most intensive flow is found in the corners, where the cylindrical surface of an activator comes in contact with the outer wall of the container (Fig. 3*a*). The flow velocity between the activators is rather weak, and a characteristic time for a fluid particle to cross the annular layer would be an order of a minute, i.e. a few tens to hundreds of oscillation periods. Vibrational convection produces a sufficiently homogeneous velocity distribution across the layer, with little stagnant zones.

By displacing the laser light sheet along the container axis it was shown that the flow pattern and fluid velocity are invariant along the z-axis. The vortices of the steady streaming are elongated parallel to the rotation axis and form regular rolls. Hence, the flow structure can be considered two-dimensional and the results obtained for one annulus cross section can be taken as representative of the whole volume.

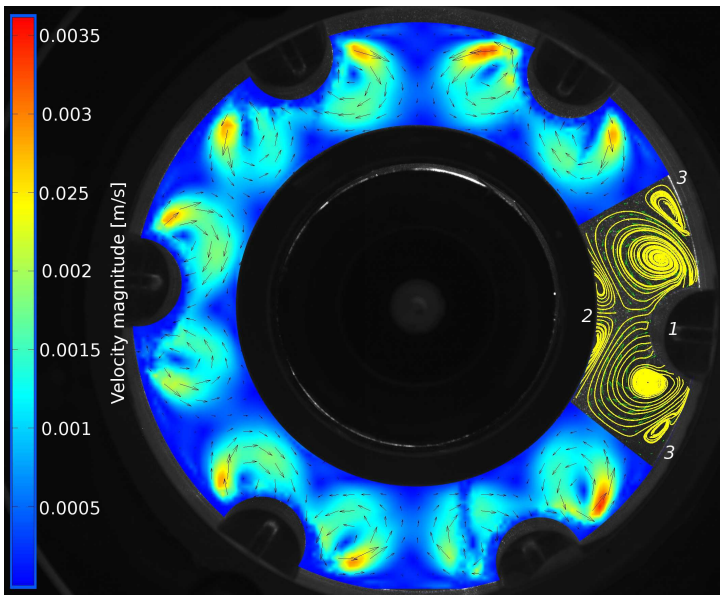

a

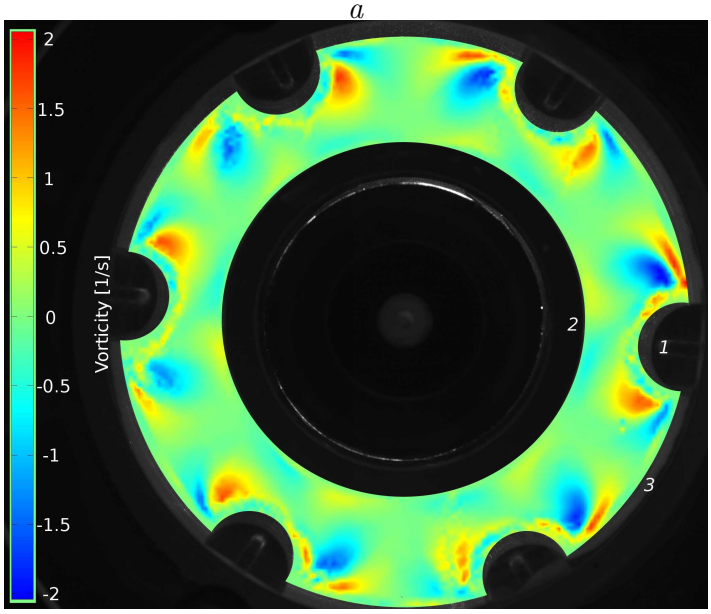

b

Figure 3. Experimental results for $f = 4.0$ Hz and $\varphi_0 = 0.050$ rad. A vector plot of the average velocity field (a) is obtained from PIV; a colour map shows the average velocity magnitude; the streamlines on the right-hand side of the figure (a) are drawn automatically as tangents to the vectors . A vorticity plot (b) is derived from the velocity field.

4.2. Numerical results

In numerical simulations the regular steady flow pattern is found, similar to that observed in experiments. The velocity magnitude in the non-viscous domain is coherent in calculations and experiments (Fig. 4). The most intensive flow is found in the viscous domain, which is rather thin so that the PIV method does not resolve it.

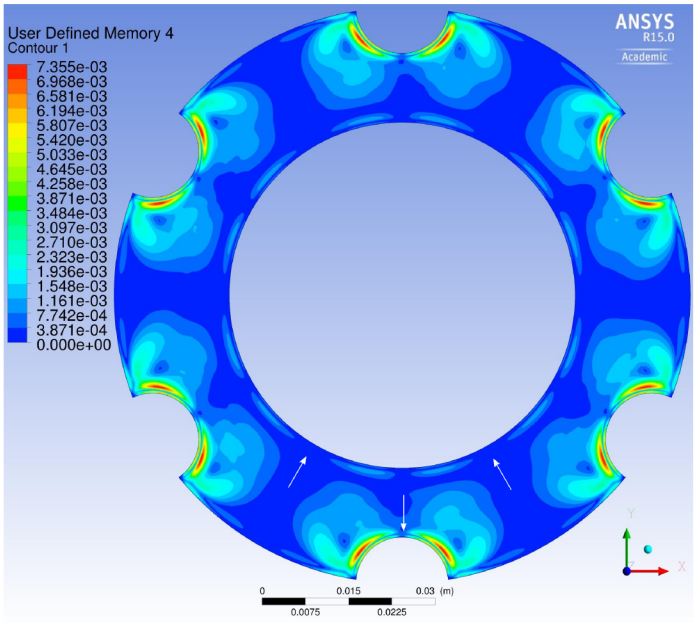

Figure 4. Colour map of the average velocity magnitude (in m/s) at $f = 4.0$ Hz, $\varphi_0 = 0.050$ rad obtained in DNS. The flow in the narrow gaps, at activators, is directed outward; in wide gaps – inward (as shown by the arrows)

The numerical method provides a good resolution in the viscous domain. Fluid oscillations generate an average vorticity in Stokes boundary layers on the activators (Fig. 5, *1*). Inside the Stokes layer the flow is directed towards the apex from both sides, and outside the boundary layer it is directed from the apex of the activator towards the wide parts of the annulus. This flow entrains the fluid in the bulk volume, thus generating secondary vortices in the non-viscous domain (Fig. 5, *2*), the same as observed in the experiment (Fig. 3, *1*). According to DNS the highest flow velocity is achieved at the distance of about 5 times the thickness of boundary layer.

The steady flow around an activator resembles closely to the steady flow around an oscillating cylinder in the form of four vortices (Schlichting 1968). Along the surface of an activator in the cross-section plane, the fluid produces tangential oscillations. The amplitude of the tangential component of pulsation velocity is not constant. It has a maximum at the activator apex, and the tangential gradient of velocity amplitude is directed towards this apex. From the theory (Schlichting 1968) it is known that the

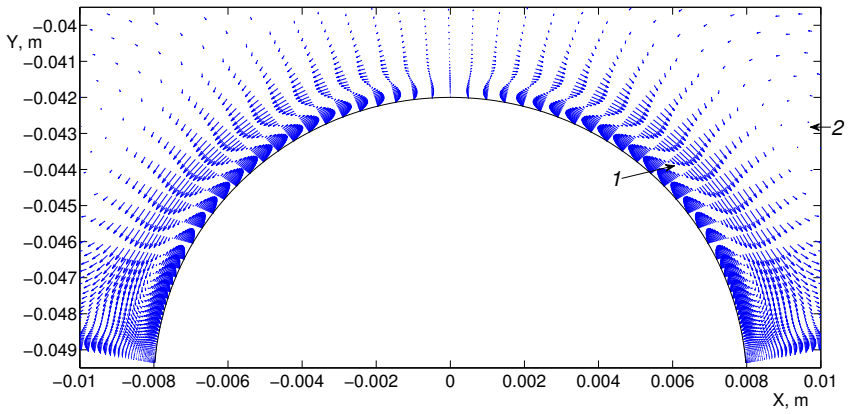

Figure 5. Vector plot of the flow near an activator at $f = 4.0$ Hz, $\varphi_0 = 0.050$ rad obtained in DNS. Two steady vortices are situated near the wall, in the viscous domain, symmetrically relative to activator apex

velocity of the secondary steady flow (outside the boundary layer) is expressed as

$$v_\tau = -\frac{3}{4\Omega} V_0 \frac{\partial V_0}{\partial x_\tau}. \tag{1}$$

Here, V_0 is the amplitude of pulsation velocity, x_τ is the coordinate tangential to the activator surface.

In Fig. 5 outside the boundary layer the flow is directed opposite the gradient $\partial V_0/\partial x_\tau$, which is in agreement with the expression (1).

5. Instability

With an increase in vibration intensity, in a threshold way the flow symmetry with respect to an activator is broken (Fig. 6). Let us call the vortices on Fig. 3, which are rotating clockwise, "even" and those rotating counter-clockwise "odd". At a critical value of vibration acceleration, $R_o\varphi_0\Omega^2$, either "even" or "odd" vortices expand beyond the activators and form a large-scale vortex encircling the inner wall in the form of a cog-wheel, let us denote it as vortex A. All of the grouped vortices have the same rotation direction, and it determines the direction of the vortex A. Meanwhile the other half of the vortices are oppressed and localized in close proximity of the activators, these vortices will be denoted as B (Fig. 6*b*).

The choice between "even" and "odd" vortices is random. For example at equal parameters, $f = 4.0$ Hz and $\varphi_0 = 0.061$ rad, in experiment (Fig. 7) and computation (Fig. 8) the opposite direction of the supercritical flow is found. The fluid velocity, excluding from consideration the viscous domain, found in the numerical simulation is in agreement with that from the experiment. Despite the opposite direction, the magnitude is the same.

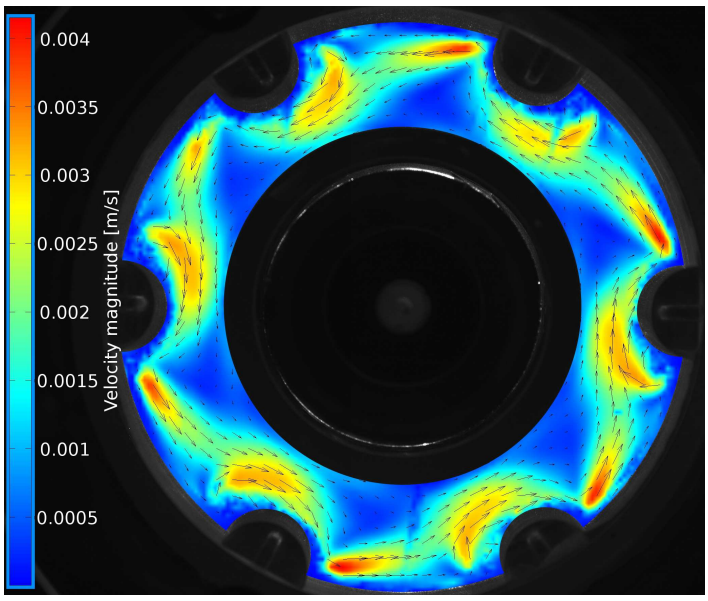

a

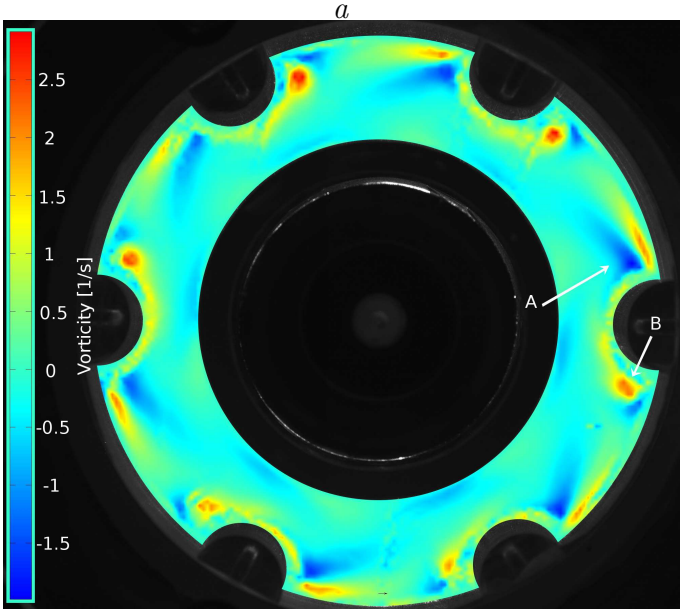

b

Figure 6. The vector plot of the average velocity (*a*) and the vorticity plot (*b*) obtained in experiment at $f = 5.0$ Hz, $\varphi_0 = 0.050$ rad. The "odd" vortices have formed a cog-wheel vortex rotating counter-clockwise, its center coincides with the container axis

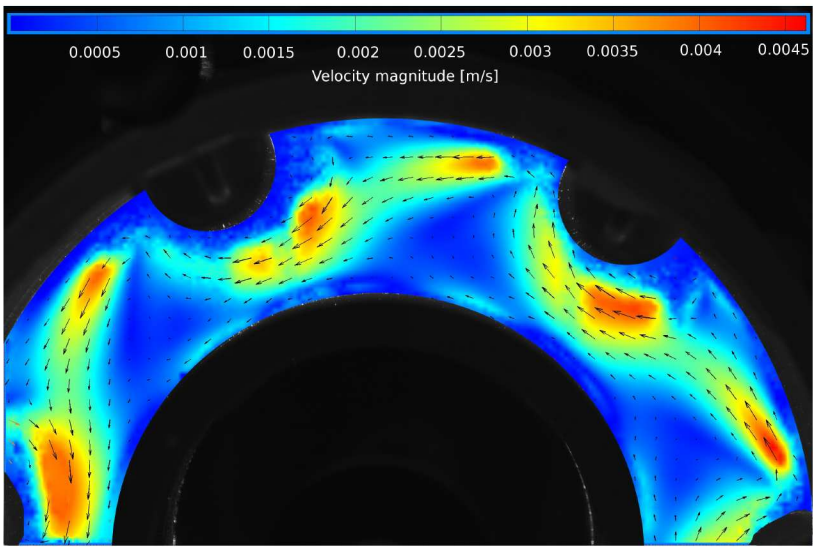

Figure 7. Colour map of the average velocity magnitude obtained in experiment at $f = 4.0$ Hz, $\varphi_0 = 0.061$ rad. A half of the annulus is shown. The "odd" vortices have formed a large-scale vortex rotating counter-clockwise

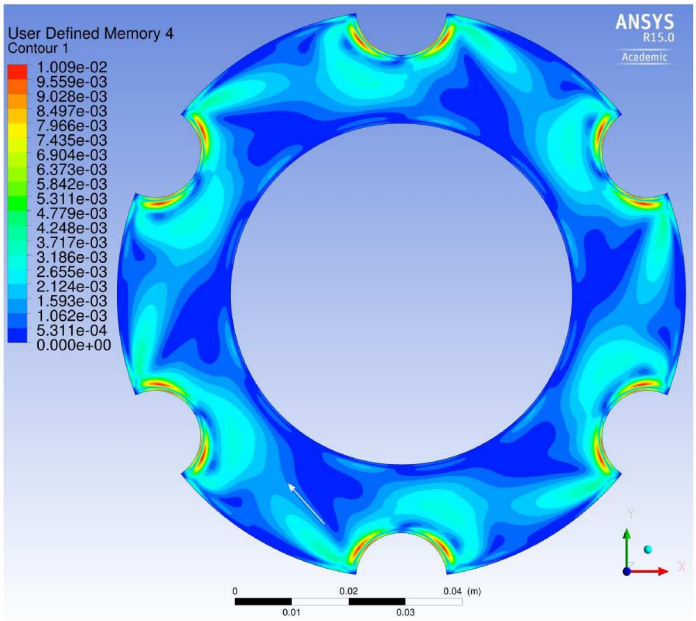

Figure 8. Colour map of the average velocity magnitude (in m/s) obtained in DNS in the case of the supercritical flow at $f = 4.0$ Hz and $\varphi_0 = 0.061$ rad. The "even" vortices have merged in a clockwise rotating cog-wheel vortex (the flow direction is shown by an arrow)

In the interior part of the cog-wheel vortex a weak motion is observed. The perimeter of the vortex A is marked with a fast, nearly uniform stream localized in the non-viscous area. The highest intensity of the non-viscous flow is found on the activators, where the large-scale vortex gets in contact with the vortices B (Fig. 7), and in the corners, where it gets in contact with the thin boundary-layer vortices. In the viscous domain the flow velocity increases with the amplitude, but no symmetry break is observed (Fig. 8).

5.1. Mechanism of instability

Following (Ivanova and Kozlov 2003), we will use for description of the studied system the following governing parameters: pulsation Reynolds number $\mathrm{Re_p} \equiv \varphi_0^2 R_o^2 \Omega/\nu$ and dimensionless frequency of oscillations $\omega \equiv \Omega R_a^2/\nu$ ($R_a = \frac{d}{2}$ is the activator radius). The first represents the ratio of the convective momentum transport to the viscous one and characterizes the vibration intensity. The second represents the squared ratio of

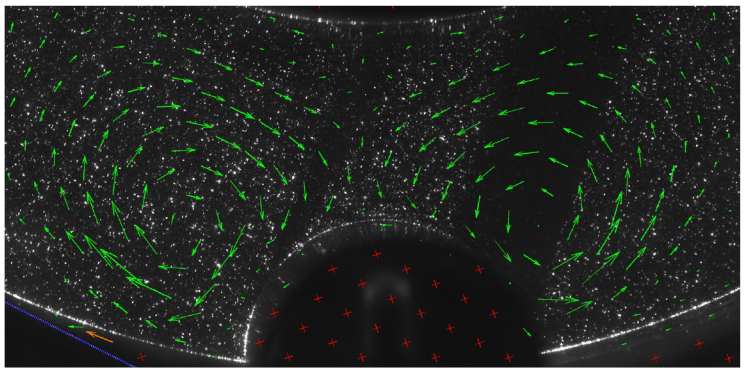

a

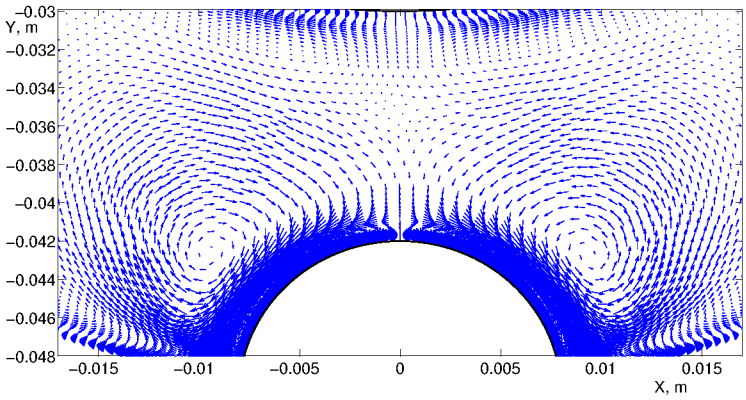

b

Figure 9. Velocity field near an activator at $f = 4.0$ Hz and $\varphi_0 = 0.04$ rad ($\mathrm{Re_p} = 101$, $\omega = 1608$); subcritical flow pattern is observed (a – experiment, $Q_a = 0.56 \pm 0.03$ mm^2/s; b – simulation, $Q_a = 0.548$ mm^2/s)

the activator radius to the thickness of a viscous boundary layer. Large values of ω

correspond to the case of low viscosity.

To characterize the activator-related symmetry of the steady streaming, a flow rate through the unit length of the activator section, cutting through the container axis and the activator apex, was calculated as

$$Q_{\mathrm{a}} = |\int_{R_{\mathrm{o}}-R_{\mathrm{a}}}^{R_{\mathrm{i}}} v_{\tau}\partial r|.$$

Here, v_{τ} is the tangential (azimuthal) projection of fluid average velocity. Since the direction of the cog-wheel vortex does not affect the velocity magnitude and simply mirrors the vectors, the flow rate is calculated as modulus.

First, let us consider the case of subcritical flow. In a narrow part of the annulus, above the activator apex, two opposite vortices get in contact and form a virtual line, along which the flow is directed towards the activator (Fig. 9). This line belongs to a radial cross-section of the annulus. In this region the tangential component of fluid velocity is small compared to the radial one. The transversal flow rate through the unit length of the radial cross-section, according to the both experiment and numerical simulation, is $Q_{\mathrm{a}} \approx 0.55$ mm^2/s. This means that for the container of 200 mm height,

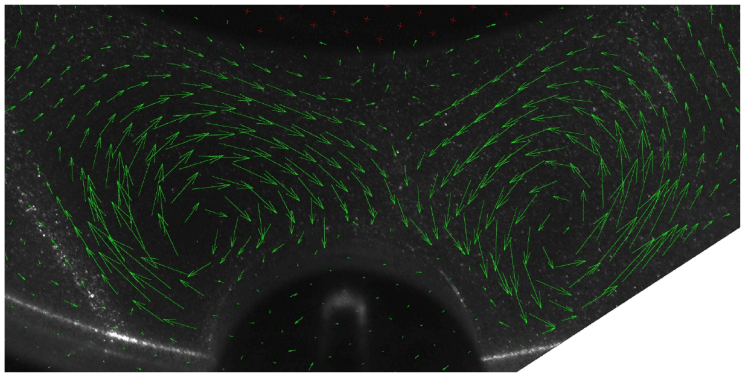

a

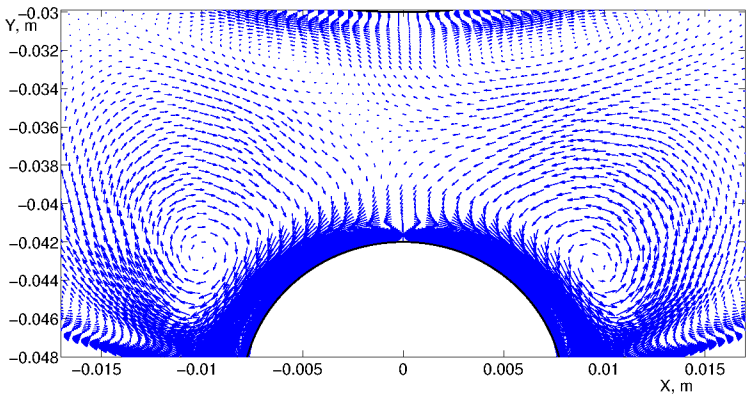

b

Figure 10. Velocity field near an activator in the stability threshold at $f = 4.0$ Hz and $\varphi_0 = 0.05$ rad ($\mathrm{Re_p} = 157$, $\omega = 1608$) (*a* – experiment, $Q_{\mathrm{a}} = 3.4 \pm 0.4$ mm^2/s; *b* – simulation, $Q_{\mathrm{a}} = 1.56$ mm^2/s)

the flow rate through the entire cross-section with the surface of 24 cm^2 is 0.11 ml/s, which is indeed a small value.

At higher vibration intensity, with increase in $\mathrm{Re_p}$, the vortices come in competition, and the flow from one of them begins sinking on the opposite side of the activator. In Fig. 10*a* the flow from the "even" vortex (on the left) enters below the "odd" vortex, while in the simulation result in Fig. 10*b* the vector plot is slightly shifted to the left witnessing of the slow transversal flow from the side of the "odd" vortex. This situation corresponds to the threshold of symmetric flow stability.

With further $\mathrm{Re_p}$ increase, a bifurcation occurs, and one of two vortices (the "odd" vortex in Fig. 11*a*) captures the flow from its opposite and grows. Its center moves away from the activator, and the excessive flow is transferred to the consecutive activator. The flow-capturing vortices thus unite in one large-scale vortex A. The vortex B in its turn is pushed closer to the activator by the flow from the vortex A.

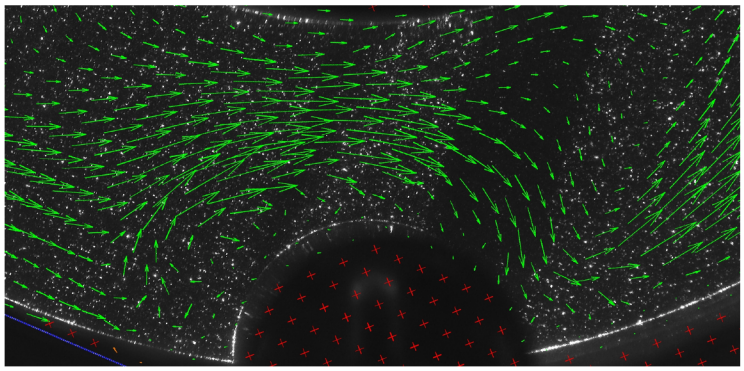

a

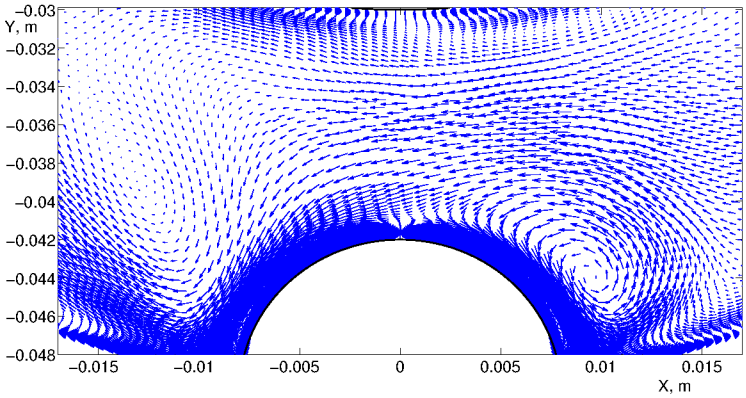

b

Figure 11. Velocity field near an activator at $f = 4.0$ Hz and $\varphi_0 = 0.06$ rad ($\mathrm{Re_p} = 226$, $\omega = 1608$); symmetry break is observed (*a* – experiment, $Q_\mathrm{a} = 21.0 \pm 0.8$ mm^2/s, the vortex B is "even"; *b* – simulation, $Q_\mathrm{a} = 15.5$ mm^2/s, the vortex B is "odd")

Comparison of Figures 9*b*, 10*b* and 11*b* reveals that the boundary-layer vortices remain symmetric relative to the activator in both subcritical and supercritical regimes.

This means that the described bifurcation may be considered as instability of the non-viscous, secondary steady flow. The vortices grow in size with $\mathrm{Re_p}$ as can be seen from comparison of Figures 9 and 10. This creates a tendency of a vortex to invade the space of its neighbouring vortex, which rotates in the opposite direction. Such situation is prone for the growth of small perturbations. And, as will be shown in Section 6, this leads to the soft onset of instability at the critical values of $\mathrm{Re_p}$ and ω.

6. Analysis

The flow stability has been studied systematically for the range of frequencies from 1 to 10 Hz, which corresponds to $\omega = 402 - 4021$. The bifurcation diagrams are presented in Fig. 12. They split according to the value of vibration frequency. The stability threshold depends on the vibration acceleration, and with the frequency increase the critical value of the amplitude φ_0 decreases (Fig. 13). The series of points in Fig. 12 are shifted along the axis φ_0 likewise. The stability threshold and the dependence of supercritical dynamics on the vibration amplitude is determined by the dimensionless frequency. This is demonstrated by a comparison of computation results for the containers of different size: $R_\mathrm{o} = 50$ mm (points *3*) and $R_\mathrm{o} = 100$ mm (*6*), meanwhile the geometrical similarity was preserved. Since the characteristic length for the points *6* was doubled, at the frequency $f = 1.0$ Hz the dimensionless frequency in this case is equal to the case of the four times higher frequency. The flow rates are equal for points *3* and *6*, as well as the threshold values of φ_0.

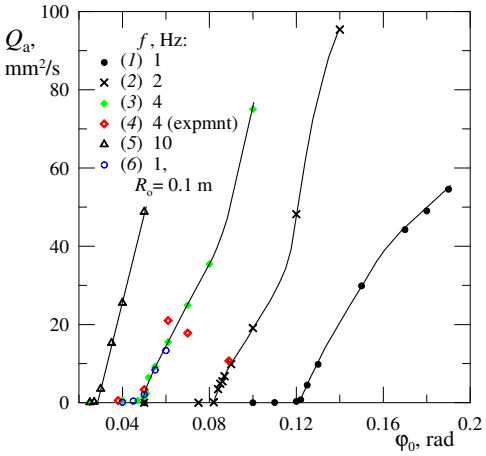

Figure 12. Bifurcation diagrams: transversal flow rate vs. amplitude. $f = 1$ Hz (*1*, *6*), 2 Hz (*2*), 4 Hz (*3*, *4*), 10 Hz (*5*). Points *4* are obtained in experiment; points *6* are calculated for $R_\mathrm{o} = 100$ mm

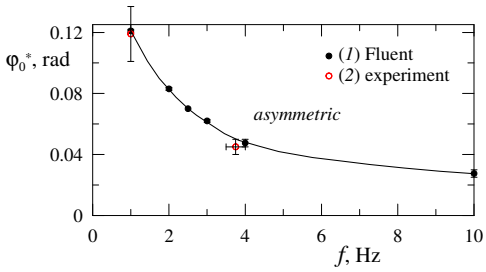

Figure 13. Stability threshold from numerical simulation (*1*) and from experiment (*2*)

Quantitative results of the experiment and the numerical simulation are in good agreement at the pulsation Reynolds number up to about 200, which corresponds to the symmetrical regime and to the moderate supercriticality. Conventionally, one can determine the latter as a condition when the average flow rate through the radial cross-section between an activator and the wall is greater than the flow rate in the threshold by about an order of magnitude. Experimental points *4* in Fig. 12 have a slight discrepancy with respect to the numerical points *3* at $\varphi \leq 0.06$ rad, but at $\varphi \geq 0.07$ rad the dependence $Q_{\mathrm{a}}(\varphi_0)$ found in experiment is completely different. PIV analysis of the flow revealed that in experiment a secondary instability occurs, at which the structure of the cog-wheel vortex is broken (Fig. 14*b*). This instability is not found in the numerical simulation, despite the wide range of parameters was studied. This means that at $\omega = 1608$, the used two-dimensional numerical model is valid for description of the flow in the container of large aspect ratio in the range $\mathrm{Re_p} < 267 \pm 41$.

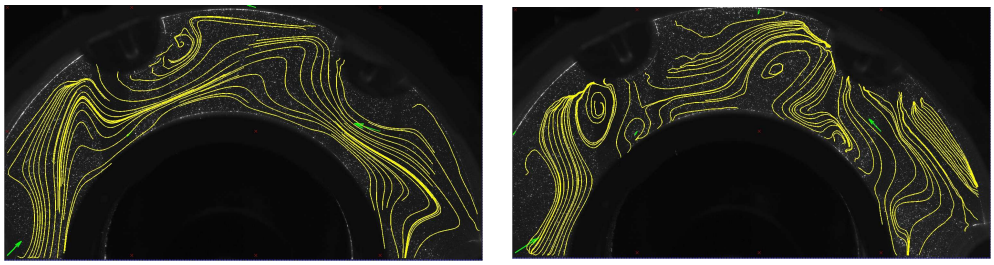

a *b*

Figure 14. Streamlines traced based on PIV data for $f = 4.0$ Hz, $\varphi_0 = 0.06$ rad (*a*) and 0.09 rad (*b*). The cog-wheel vortex is regular in figure (*a*), at the higher amplitude it undergoes an instability (*b*)

In order to compare the results at different values of the dimensionless frequency ω, we introduce a dimensionless flow rate $(Q_{\mathrm{a}}/\nu)\,\omega$. The points series split according to the dimensionless frequency, and it is possible to follow the evolution of the dependency with ω increase (Fig. 15). At $\omega = 402$ (points *1*) the dimensionless flow rate grows with $\mathrm{Re_p}$ by a logarithmic law. At $\omega = 4021$ (points *5*) this dependence is very close to linear. The curves interpolating the series at $\omega = 804$ (points *2*) and at $\omega = 1608$ (points *3*–*6*) have a transient shape. If now we consider the threshold of symmetric flow stability, the studied range of ω lies between two asymptotic limits, in which $\mathrm{Re_p}$ does not depend on ω (Fig. 16). This explains that the transition of the dependence of $(Q_{\mathrm{a}}/\nu)\,\omega$ on $\mathrm{Re_p}$ from logarithmic to linear is associated with the transition between two limiting cases.

The instability of secondary steady flow in the limit of high ω was reported by Ivanova & Kozlov (2003). They experimentally studied the dynamics of fluid flow in a rotationally vibrating cylinder of the square cross-section. In this case a steady streaming in the form of eight vortices is generated. In each corner of the square cross-section, a pair of vortices with opposite circulation are located. With an increase in $\mathrm{Re_p}$, a half of vortices with the same rotation direction are united in one large-scale vortex,

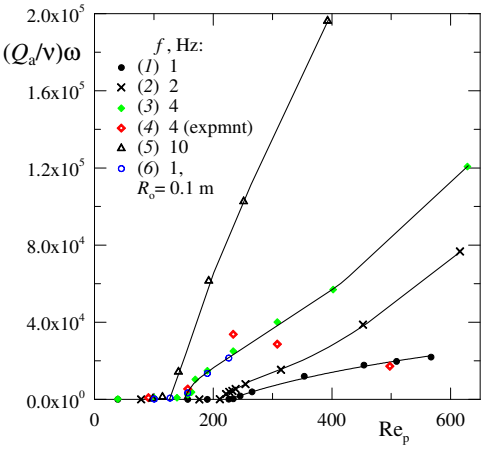

Figure 15. Bifurcation diagrams on the plane of dimensionless parameters. Notations correspond to Fig. 12

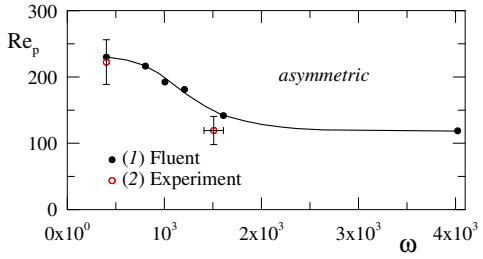

Figure 16. Stability threshold on the plane of dimensionless parameters $(\omega, \mathrm{Re_p})$, *1* – DNS, *2* – experiment. At extremities of the studied range of ω the points approach two asymptotic values of $\mathrm{Re_p}$

while the other four vortices are pushed towards the container walls. At $\omega > 5000$ the flow is self-similar with respect to the frequency; here ω is calculated from the half of the lateral size of the square $a/2$ as the length scale. In this limiting case the subcrical and supercritical flow velocity, as well as the symmetry break threshold, are determined uniquely by the pulsation Reynolds number. In the work by Ivanova & Kozlov (2003) the rotation rate of the large-scale vortex is proportional to $\mathrm{Re_p}$. This qualitatively agrees with the results of the present research for high ω (Fig. 15, points *5*).

7. Conclusion

The flow excited by rotational vibrations in an annulus with deflectors has been studied experimentally and numerically. Tangential oscillations of the deflectors lead to the generation of the steady streaming in the Stokes boundary layers. The secondary steady flow establishes in the whole volume of the annulus. The flow pattern is a regular system of two-dimensional vortices with alternating rotation direction, each pair of vortices being symmetric with respect to an activator.

With an increase in the vibration intensity the secondary steady flow undergoes an instability, and the vortices with the same rotation direction merge in one large-scale cog-wheel vortex, while their opposites are reduced in size and pushed closer to the activators. Thus, the activator-wise symmetry is broken. The instability occurs because at the higher forcing acceleration the neighbouring vortices become too big and invade the space of their respective neighbours.

The results obtained in experiment and in DNS are in good agreement below the symmetry-break threshold, and above it if the forcing is not high. Above a certain value of the pulsation Reynolds number ($\mathrm{Re_p} = 267 \pm 41$ at $\omega = 1608$), in the experiment a

secondary instability is observed, which has not been found in the numerical simulation. This regime of higher supercriticality remains an open topic for study.

Stability threshold is governed by two parameters: the dimensionless frequency ω and the pulsation Reynolds number $\mathrm{Re_p}$. With increase in ω the critical value of $\mathrm{Re_p}$ decreases. At the extremities of the studied range of frequencies the dependency $\mathrm{Re_p}\,(\omega)$ tends to become asymptotic.

In the limiting case of high frequencies, a qualitative agreement is found with an earlier research done by other authors for rotationally oscillating container with the square cross-section. The law, by which the rotation rate of the cog-wheel vortex grows with $\mathrm{Re_p}$, tends to become linear at the highest ω.

Acknowledgments

The work was supported by the Ministry of Education of Permskii Krai (project C-26/625) and by the Ministry of Education of Russian Federation (task 2014/372, project 2176).

References

Batchelor, G. K. 1970 *An Introduction to Fluid Dynamics*, Cambridge University Press.

Blechman, I. I. 2003 *Vibrational Mechanics*, Allied Publishers, New Delhi, isbn 9788177644579.

Honji, H. 1981 *Streaked flow around an oscillating circular cylinder*, J. Fluid Mech. **107**, 509–520.

Ivanova, A.A. and Kozlov, V.G. 2003 *Vibrational Convection in a Nontranslationally Oscillating Cavity (Isothermal Case)*, Fluid Dyn. **38**, 186–192.

Ivanova, A. A., Kozlov, V. G., Polezhaev, D. A., Pareau, D. and Stambouli, M. 2009 *Heat Transfer in a Closed Cavity under Conditions of Forced Vibrational Convection*, Fluid Dynamics **44(4)**, 481–489.

Kola, A., Ye, Y., Ho, A., Le-Clech, P. and Chen, V. 2012 *Application of low frequency transverse vibration on fouling limitation in submerged hollow fibre membranes*, Jl. of Membrane Science **409–410**, 54–65.

Kumar, H., Tawhai, M. H., Hoffman, E. A. and Lin, C.-L. 2011 *Steady streaming: A key mixing mechanism in low-Reynolds-number acinar flows*, Phys. Fluids **23**, 041902.

Riley, N. 2001 *Steady Streaming*, Ann. Rev. Fluid Mech. **33**, 43–65.

Schlichting, H. 1932 *Berechnung ebener periodischer Grenzschichtströmungen*, Phys. Z. **33**, 327–335.

Schlichting, H. 1968 *Boundary-layer Theory*, McGRAW-HILL, New-York (re-edited in 1979).

Stuart, J. T. 1966 *Double boundary layers in oscillatory viscous flow*, J. Fluid Mech. **24**, 673–687.

Tatsuno, M. and Bearman, P. W. 1990 *A visual study of the flow around an oscillating circular cylinder at low Keulegan-Carpenter numbers and low Stokes numbers*, J. Fluid Mech. **211**, 157–182.

Thielicke, W. and Stamhuis, E. J. 2014 *PIVlab – Towards User-friendly, Affordable and Accurate Digital Particle Image Velocimetry in MATLAB*, Journal of Open Research Software **2**(1):e30.